

Bis(arylvinyl)pyrazines, -pyrimidines, and -pyridazines As Imaging Agents for Tau Fibrils and β -Amyloid Plaques in Alzheimer's Disease Models

Alexander Boländer,[†] Daniel Kieser,[†] Constantin Voss,[†] Silvia Bauer,[†] Christian Schön,[‡] Steffen Burgold,[‡] Tobias Bittner,[‡] Jana Hölzer,[§] Roland Heyny-von Haußen,^{||} Gerhard Mall,^{||} Valérie Goetschy,[⊥] Christian Czech,[⊥] Henner Knust,[⊥] Robert Berger,[†] Jochen Herms,[‡] Ingrid Hilger,[§] and Boris Schmidt^{*,†}

[†]Clemens Schoepf-Institute of Organic Chemistry and Biochemistry, Technische Universität Darmstadt, Petersenstrasse 22, 64287 Darmstadt, Germany

[‡]DZNE site Munich and Center of Neuropathology, Ludwig-Maximilians-Universität, 81377 Munich, Germany

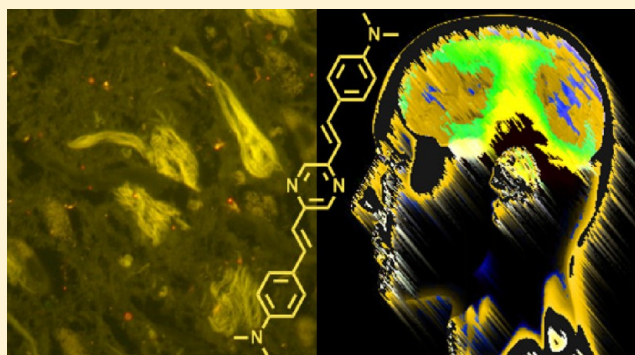
[§]Institute of Diagnostic and Interventional Radiology I, Experimental Radiology, Universitätsklinikum Jena, 07747 Jena, Germany

^{||}Department of Pathology, Klinikum Darmstadt, 64287 Darmstadt, Germany

[⊥]F. Hoffmann-La Roche AG, CH-4070 Basel, Switzerland

S Supporting Information

ABSTRACT: The *in vivo* diagnosis of Alzheimer's disease (AD) is of high socioeconomic interest and remains a demanding field of research. The biopathological hallmarks of the disease are extracellular plaques consisting of aggregated β -amyloid peptides ($A\beta$) and tau protein derived intracellular tangles. Here we report the synthesis and evaluation of fluorescent pyrazine, pyrimidine, and pyridazine derivatives *in vitro* and *in vivo* aiming at a tau-based diagnosis of AD. The probes were pre-evaluated on human brain tissue by fluorescence microscopy and were found to label all known disease-related alterations at high contrast and specificity. To quantify the binding affinity, a new thiazine red displacement assay was developed and selected candidates were toxicologically profiled. The application in transgenic mouse models demonstrated bioavailability and brain permeability for one compound. In the course of histological testing, we discovered an AD-related deposition of tau aggregates in the Bowman's glands of the olfactory epithelium, which holds potential for an endoscopic diagnosis of AD in the olfactory system.



■ INTRODUCTION

With approximately 36 million people worldwide suffering from dementia and with that number expected to grow to 114 million by 2050, AD is the most common type of dementia among older adults.¹ There is no cure for the disease, and a distinct diagnosis can be carried out by postmortem examination only, when the biopathological hallmarks of AD are detectable in human brain tissue. These are two notorious protein aggregates: extracellular plaques mainly consisting of two β -amyloid peptides $A\beta_{40}$ and $A\beta_{42}$ and intracellular tangles resulting from the aggregation of abnormally hyperphosphorylated tau protein to paired helical filaments. Both deposits are considered to impair intra- and interneuronal reaction cascades, causing progressive neurodegeneration almost decades before the first signs of cognitive impairment emerge.² It has been shown that the load of tau fibrils in brain tissue correlates far more accurately to the severity of dementia, whereas there are several reports for amyloid plaque burden at autopsy, yet no signs of cognitive impairment during lifetime.³ Nevertheless,

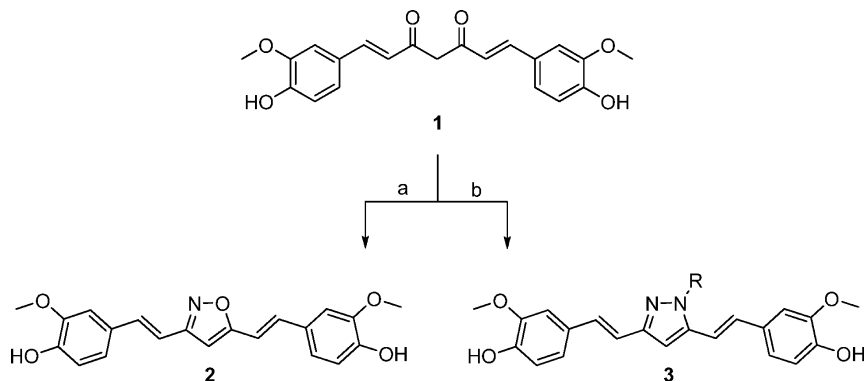
both deposits remain the most important targets for *in vivo* imaging of disease progression. Especially positron emission tomography (PET) and single photon emission computed tomography (SPECT) are under constant further development with respect to new radiolabeled markers to visualize the pathology. [¹¹C]PIB is the most prominent and most frequently applied PET tracer to visualize $A\beta$ *in vivo*.⁴

The insufficient ability of the markers to discriminate between intracellular tau and extracellular $A\beta$ and the relative amounts of these deposits limit them to $A\beta$ detection. In the course of ligand design, tau-targeting probes have emerged more slowly than $A\beta$ probes. This may be due to the still overwhelming interest in $A\beta$. Therefore tau-directed probes are needed. On the basis of histological staining of tau fibrils and

Special Issue: Alzheimer's Disease

Received: May 9, 2012

Published: August 22, 2012

Scheme 1. Reported Synthesis of Curcumin-Derived Isoxazoles 2 and Pyrazoles 3^a

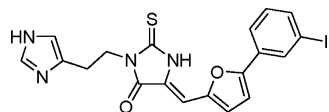
^a(a) $\text{NH}_2\text{OH}\cdot\text{HCl}$, pyridine, EtOH, reflux. (b) RNHNH_2 , MeOH, NEt_3 , rt/ RNHNH_2 , trifluoroacetyl (TFA), toluene, reflux.⁵

$\text{A}\beta$ plaques, we sought nontoxic fluorescent dyes of high photostability and a high affinity to tau over $\text{A}\beta$, easy to handle and applicable in biological and histological staining.

RESULTS AND DISCUSSION

We reported on curcumin-derived isoxazoles 2 and pyrazoles 3 as high-affinity ligands for fibrillar $\text{A}\beta_{42}$ aggregates and as potent inhibitors of tau aggregation recently (Scheme 1).

These results suggest a fundamental affinity of these compounds to tau deposits in vitro. The same rationale was exploited to arrive at the tau ligand TH-2 (4) (Figure 1).⁶



TH-2 (4)

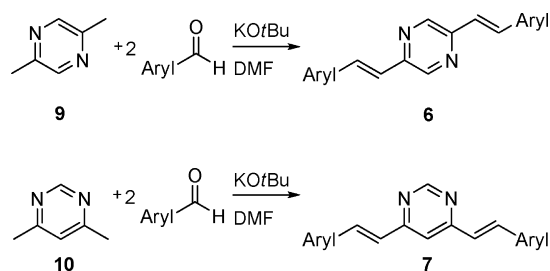
Figure 1. Structure of the tau ligand TH-2 (4).⁶

Curcumin (1) itself is currently used in optical imaging studies and led to the identification of $\text{A}\beta$ plaques in the mouse retina, yet it requires high intravenous dosage of 1, which is deemed toxic for humans.⁷ Unfortunately, the fluorescence of isoxazoles 2 and pyrazoles 3 is low, and their derivation from 1 imposes limits on the substitution pattern of their phenyl-enevinylene flanks. Structurally, they resemble methoxy-XO4 (5) (Figure 2), the benchmark ligand for fluorescence microscopy of $\text{A}\beta$ plaques in vivo, which has also been used for $\text{A}\beta$ -PET imaging as its ¹¹C-labeled isotopologue⁸ but displays very low clearance and nonideal single-photon excitation in tissue, ruling out a clinical application.^{8–10}

The replacement of the anisole core of 5 by pyrazine, pyrimidine, or pyridazine as aromatic cores with a high electron-withdrawing character and significant aromaticity should lead to molecules with high conjugation length and permits a large structural variability within the flanks of the molecule. This allows for an improvement of physicochemical properties by introducing functional groups affecting lipophilicity and fluorescence. Herein we describe the synthesis of bis(arylviny)pyrazines 6, -pyrimidines 7, and -pyridazines 8 (Figure 2) and their histological and toxicological evaluation with respect to AD pathology, aiming at an in vivo diagnosis of AD-associated protein deposits.

The styryl scaffold of 6 and 7 is formed in an atom-efficient reaction by the condensation of aromatic aldehydes and dimethylpyrazine 9 or dimethylpyrimidine 10 according to a slightly modified published procedure (Scheme 2).¹¹

Scheme 2. Synthesis of Bis(arylviny)pyrazines 6 and -pyrimidines 7



The selectivity was sufficiently high to generate *trans* isomers only within the limits of NMR detection by the coupling

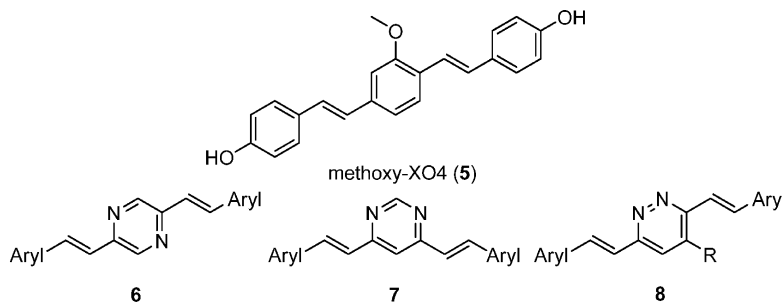


Figure 2. 5, bis(arylviny)pyrazines 6, -pyrimidines 7, and -pyridazines 8.

Table 1. 5 and the Synthesized Bis(arylviny)pyrazines 6a–h, -pyrimidines 7a–f, and -pyridazines 8a–e with Determined Affinities, Spectroscopical Data, and Polarizability

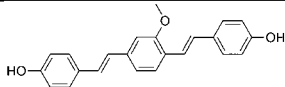
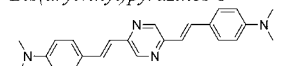
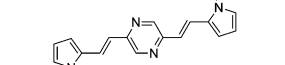
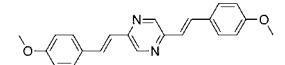
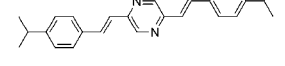
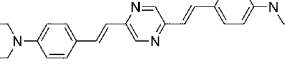
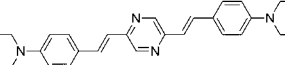
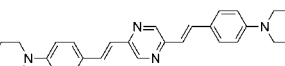
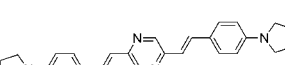
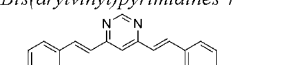
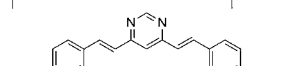
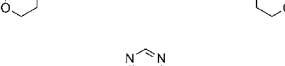
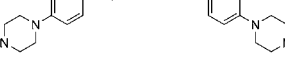
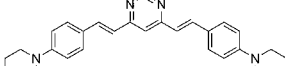
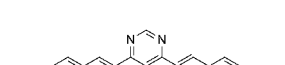
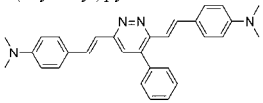
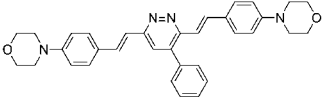
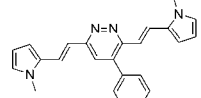
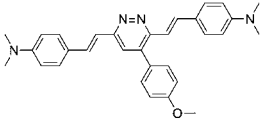
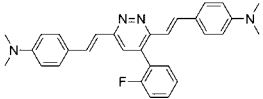
compound	IC ₅₀ (nM) ^a		cLogP ^b	λ _{abs} ^{max} (nm)	λ _{abs} ^{max} (nm) (calculated) ^c	λ _{em} ^{max} (nm)	α' (a ₀ ³) ^d
	Tau	Aβ					
5 	246	140	5.35				
<i>Bis(arylviny)pyrazines 6</i>							
6a 	<i>n.m.</i> ^e		4.10	405	453	570	507
6b 	<i>n.m.</i> ^e		1.38	435	420	544	362
6c 	13	17	3.89	380	414	486	421
6d 	<i>inactive</i>		6.29	375	403	457	455
6e 	6	43	2.87	380	448	564	560
6f 	42	51	3.12	390	454	556	608
6g 	<i>n.m.</i> ^e		5.29	385	454	574	585
6h 	<i>n.m.</i> ^e		4.66	416	458	565	568
<i>Bis(arylviny)pyrimidines 7</i>							
7a 	4	54	4.54	430	428	575	462
7b 	<i>inactive</i>		3.32	380	424	538	517
7c 	7469	2381	3.56	405	427	552	563
7d 	17	156	5.73	414	429	576	540
7e 	2	52	5.10	440	434	581	522
7f 	2	3	5.68	450	476	587	635

Table 1. continued

compound	IC ₅₀ (nM) ^a		cLogP ^b	λ _{abs} ^{max} (nm)	λ _{abs} ^{max} (nm) (calculated) ^c	λ _{em} ^{max} (nm)	α' (a ₀ ³) ^d	
	Tau	Aβ						
<i>Bis(arylviny)pyridazines 8</i>								
8a		<i>inactive</i>	6.13	411	455	537	559	
8b		4707	7591	4.91	365	448	535	614
8c		<i>inactive</i>	3.41	409	429	509	419	
8d		1591	4571	5.96	410	453	534	580
8e		1251	10066	6.19	415	457	535	560

^aIC₅₀ values were determined in a thiazine red displacement assay as duplicates of replicate experiments.¹³ ^bCalculated cLogP values.¹⁴ ^cCalculated absorption maxima.¹³ ^dCalculated static electronic polarizability volume $\alpha' = \alpha / (4\pi\epsilon_0)$ in units of the Bohr radius cubed (a_0^3), where α = calculated polarizability¹³ and ϵ_0 = vacuum permittivity.¹³ ^en.m.: not measurable due to spectral overlap with the reference compound thiazine red.

constant for the vinylic protons in the ¹H NMR spectra (*J* ca. 16 Hz). The products obtained are listed in Table 1.

The synthesis of the bis(arylviny)pyridazines **8** was carried out via a 10-step synthesis (Scheme 3).

Starting from glycine ethyl ester hydrochloride **11**, tetrazinedimethylcarboxylate **12** was obtained according to a strategy reported for **13a** (R = phenyl).¹² The diversity of the aromatic substituent R on the pyridazines **14a–c** was introduced by a subsequent Diels–Alder reaction with inverse electron demand utilizing **12** and the aromatic alkynes **13a–c** to provide novel derivatives.

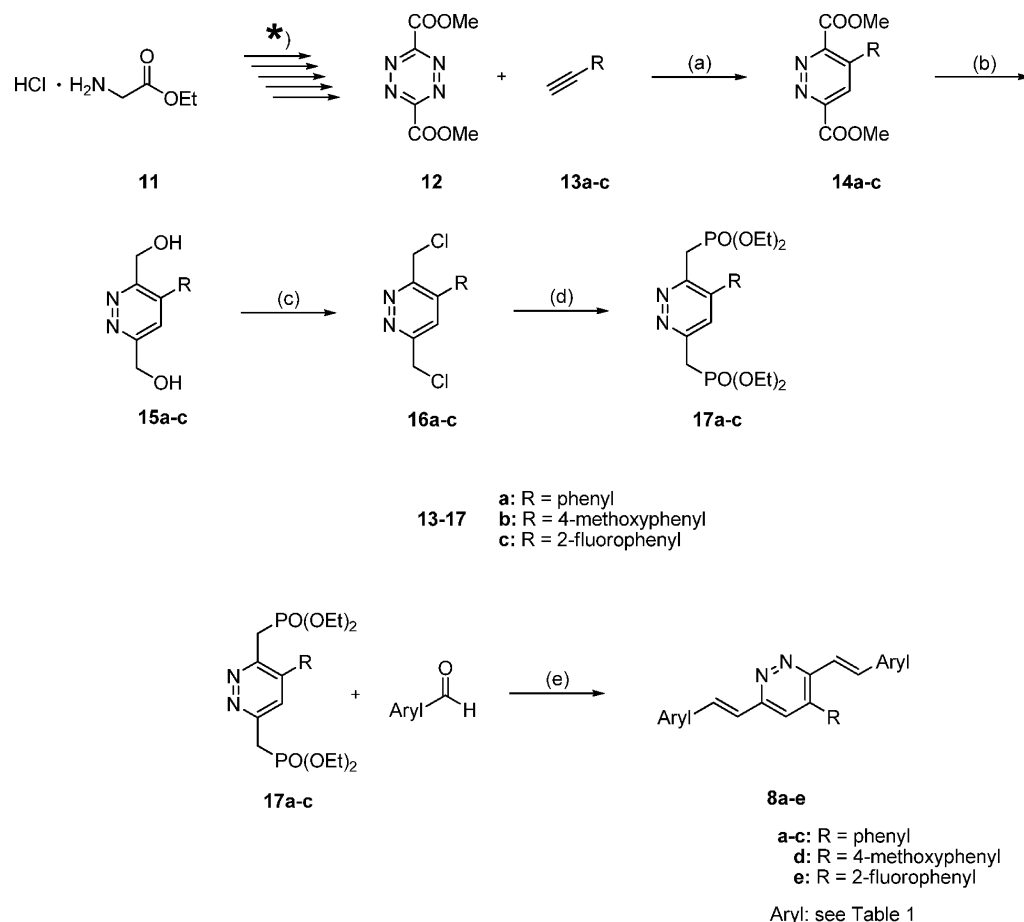
Reduction of **14a–c** and conversion of the resulting dialcohols **15a–c** yielded 3,6-bis(chloromethyl)pyridazines **16a–c**. From the latter resulted the corresponding diphosphonates **17a–c** that underwent a Horner–Wadsworth–Emmons reaction with aromatic aldehydes to yield the desired bis(arylviny)pyridazines **8a–e** (Table 1).

For all compounds we calculated¹³ the absorption maxima and determined the absorption and emission maxima in solution. In a preliminary in vitro study, the synthesized dyes were applied to human brain tissue with AD pathology.¹⁵ The affinity to tau fibrils and Aβ plaques was evaluated qualitatively by fluorescence microscopy.¹³ All of the tested compounds showed good to excellent staining of both tau fibrils and Aβ plaques at high contrast, low background staining, and high photostability in accord with immunohistochemical staining applying the antibodies anti-PHF-Tau clone AT8 mAb for tau deposits and amyloid A4 for Aβ plaques (Figure 3A–D).

Though staining with antibodies is still the generally accepted benchmark to evaluate new imaging markers, antibodies often display a lack of sensitivity. AT8-staining fails to detect up to 38% of neurofibrillary tangles.¹⁶ Especially so-called ghost tangles, which are released from affected neurons after cell-degeneration and are typical of late stages of AD, do not show any positive immune-tau-staining.¹⁷ Indeed the detection of ghost tangles is of high interest if it comes to a *postmortem*

classification of the stage of AD at hand. They may be identified by immunostaining of ubiquitin, a polypeptide, which is also a part of neurofibrillary tangles. Because ubiquitin is expressed in all eukaryotic cells, it is not a specific indicator however.¹⁸ Our ligands stain both intracellular fibrillar threads of tau and apparent extracellular aggregates of tau (Figure 3E). In addition to extracellular Aβ plaques, brain matter affected by AD pathology harbors additional amyloid deposits within the vascular walls of blood vessels called Aβ-angiopathies, which are also considerably stained by **6a** (Figure 3F).¹⁹ The primary screen on human AD brain preparations filtered test compounds for tau-staining properties. Eventually all tau positives also stained amyloid plaques, yet at variable degree. Thus, all AD-related pathological protein deposits are stained by our dyes in a one-time procedure and can be detected by fluorescence microscopy. One example is provided in Figure 3.¹³

Histological in vitro staining experiments provide little information on absolute affinities and are not directly comparable with respect to prospective in vivo imaging. Thus, we developed a new in vitro affinity assay to determine the IC₅₀ values versus thiazine red displacement from aggregated tau and Aβ₄₀.¹³ Thiazine red was selected as reference marker because it was previously shown to be an accurate marker for β-pleated sheet structures and to reliably stain Aβ plaques, tau fibrils, and diffuse neurofibrillary tangles (*K_d* for aggregated tau = 18 nM, *K_d* for aggregated Aβ = 49 nM).^{13,16,20,21} We evaluated the established Aβ marker **5** in this assay. ¹¹C-labeled **5** was reported to display an affinity of *K_i* = 26.8 nM to aggregated Aβ₄₀ in a displacement assay versus unlabeled **5**.⁸ In our assay it turned out to be a much weaker ligand in competition to thiazine red, displaying an IC₅₀ of 140 nM on Aβ₄₀. All IC₅₀ values are listed in Table 1. Almost all of our compounds show higher affinity to aggregated tau than to Aβ₄₀, except for **7c**. Even though **5** is considered a selective amyloid marker, we could only determine a 1.8-fold higher

Scheme 3. Synthesis of Bis(arylvinyl)pyridazines 8^a

^a(*) Five-step synthesis of tetrazinedimethylcarboxylate **12** according to a published procedure¹² and further five-step conversion of **12** to bis(arylvinyl)pyridazines **8a–e**: (a) dioxane, reflux; (b) LiAlH₄, 60 °C; (c) SOCl₂, CH₂Cl₂, rt; (d) P(OEt)₃, 110 °C; (e) NaH, dimethylformamide (DMF), rt.

affinity to A β over tau. It is reported that the relative amounts of amyloid and tau deposits require a 20- to 50-fold higher selectivity toward tau to allow in vivo detection of tau. Compounds that do not reach this threshold are limited to the detection of tau in the entorhinal cortex.²² If it comes to tau-selective markers, **7e** meets this criterion. **7a** has a comparable tau affinity; however, it is just 13.5-fold higher than its A β affinity. Caveat: This selectivity was observed in in vitro assays, which may not reflect the physiological situation in vivo.

A distinct structure–activity relationship cannot be deduced from the affinity results. The variable substituents of the tested molecules do not solely account for a probe's affinity, although a trend can be observed indicating that *N*- or *O*-containing substituents in the para position on the aromatic flanks drastically increase affinity. Nevertheless, they do not guarantee high affinity; both shape and size of the entire molecule seem to provide an equipotent influence: **6e** shows a very high affinity to aggregated tau (IC₅₀ = 6 nM) and a moderate one to A β ₄₀ (IC₅₀ = 43 nM). Its angular isomer **7b** shows no notable affinity to tau or A β ₄₀ at all. **8b** has a nearly linear equilibrium structure in its electronic ground state; the additional phenyl ring on the pyridazine core buckles the angle between the 4-morpholinostyryl branches marginally but significantly enlarges the size of the molecule, which seems to strongly diminish its target affinity (aggr. tau IC₅₀ = 4707 nM, aggr. A β ₄₀ IC₅₀ = 7591 nM). This observation is valid for all tested bis(arylvinyl)-

phenylpyridazines **8**. They all show an extremely low target binding. Where a direct comparison is possible, bis(arylvinyl)pyridazines **6** show higher affinities than their bis(arylvinyl)pyrimidine isomers **7**. On the other hand, angular bis(arylvinyl)pyrimidines **7** can show high to excellent affinity, especially **7a**, **7e**, and **7f**. Because a general correlation between substitution pattern and affinity does not seem to exist, we tried to correlate affinities to physicochemical parameters, starting with the calculated cLogP values (Table 1). We clearly emphasize that these values are obtained from calculations based on specific algorithms for calculating cLogP from fragment-based methods and can differ from experimental determinations by a value of 2–3.¹⁴ (For **5** the calculated cLogP value is 5.35 whereas the experimentally determined value is reported as 2.6).⁸ The plotting of the IC₅₀ values against the cLogP values indicates a lack of exploitable correlation.¹³

Besides, polarizability has been proposed as a descriptor for tau binding affinity within individual scaffold families.²³ Inspired by these results, we calculated the static electronic polarizabilities α' of our compounds (Table 1) and plotted the corresponding IC₅₀ values against them.¹³ Again, there is no significant correlation between polarizability and affinity of this ligand series to tau and A β .¹³ Because of the poor correlation of both cLogP and static electronic polarizability α' to both tau and A β affinity, neither parameter seems useful for further

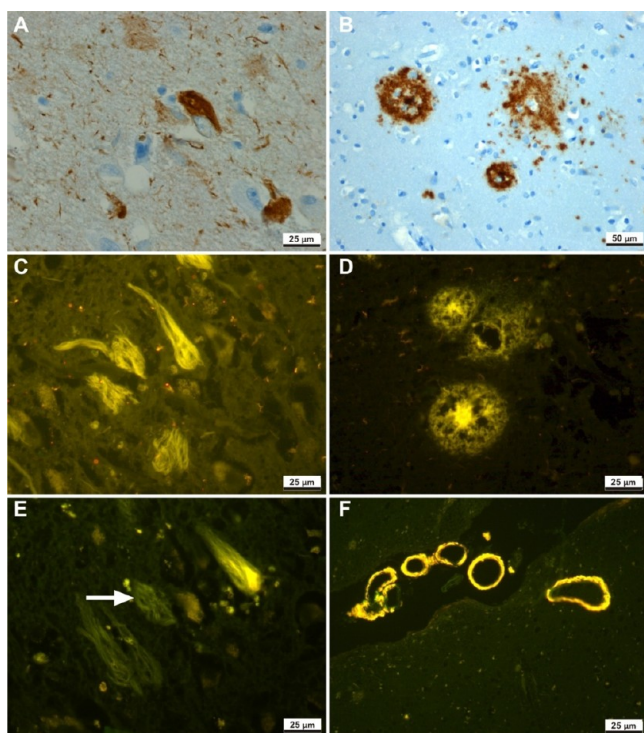


Figure 3. AD-related deposits on human brain tissue: (top) immunohistologically stained tau fibrils with antibody AT8 mAb (A) and $A\beta$ plaques with antibody amyloid A4 (B); (middle) tau fibrils (C) and $A\beta$ plaques (D) stained with **6a**; (bottom) intracellular tau tangle and extracellular tau tangles (arrow-marked) (E) and $A\beta$ angiopathy (F) stained with **6a**.¹⁵

improvement of our markers. Because **7a** and **7e** show the highest affinity to aggregated tau (**7a**, $IC_{50} = 4$ nM; **7e**, $IC_{50} = 2$ nM) over a moderate $A\beta$ affinity (**7a**, $IC_{50} = 54$ nM; **7e**, $IC_{50} = 52$ nM), we decided to test both compounds in vivo. After the toxicological evaluation in human liver carcinoma cell lines, Hep G2 did not show any significant decline in cell vitality. We evaluated selected candidates in vivo in a transgenic mouse model.^{13,24} However, recent in vivo studies and histological staining experiments indicate severe discrepancies between labeling experiments of human and murine tau, which refers to significant conformational differences between the two, and suggest the absence of the appropriate ligand-binding sites on transgenic murine tau versus human tau aggregates.²⁵ Thus, we relied on the $A\beta$ affinity of both ligands to determine the brain permeability and bioavailability in a transgenic mouse model overexpressing $A\beta$ ($APP_{swe}PS1_{\Delta E9}$) and equipped with a cranial window. Although **7e** did not show any positive results, $A\beta$ plaques were very well detectable with **7a** in the mouse brain by in vivo fluorescence microscopy 4 h after injection of 2 mg/kg (Figure 4A). Counterstaining with **5** was performed in the same mouse 2 days later by the additional injection of 2 mg/kg and confirmed the results as the areas stained by **7a** were overlaid by the areas stained by **5** (Figure 4B).

The fluorescence properties of **7a** in solution are characterized by a broad excitation range and a remarkable Stokes shift of about 140 nm (Figure 5A). The emission of **7a** after target binding shows a maximum at 510 nm, which enables for an easy distinction from stained lipofuscin deposits at 570 nm, whose accumulation is also implicated in several neurodegenerative diseases (Figure 5B and C).²⁶

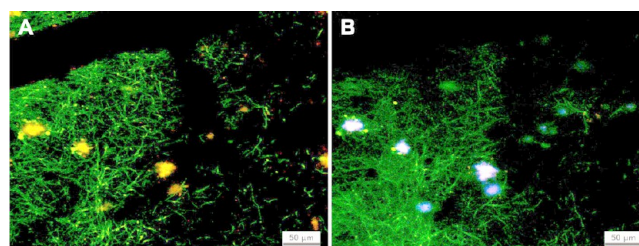


Figure 4. (A) Detection of $A\beta$ plaques stained with **7a** in $APP_{swe}PS1_{\Delta E9}$ transgenic mouse model (2 mg **7a**/kg intraperitoneal injection (ip) after 4 h) through cranial window in vivo. (B) Counterstaining by additional injection of **5** in the same mouse on day 2 (2 mg **4**/kg ip after 4 h).^{13,24}

CONCLUSION AND OUTLOOK

In summary, we present a series of fluorescent probes for in vitro detection of AD-associated protein deposits in human brain tissue by fluorescence microscopy, offering a broad excitation and emission range by the choice of suitable candidates. Two of these compounds (**7a** and **7e**) even show a remarkably higher selectivity for aggregated tau, which qualifies for further tau-selective imaging techniques with respect to an early-onset diagnosis of AD. The ability of **7a** to pass the blood–brain barrier was demonstrated in a transgenic mouse model by the $A\beta$ binding of that compound in vivo. In the course of our histological studies of ligand profiling on human AD-altered brain material, we discovered that certain areas of the olfactory epithelium, which can be considered an extension of the brain actually, harbor tau deposits.^{13,15} These are the Bowman's glands, which are involved in the production of nasal discharge but also contain nerve tissue (Figure 6B–D). Our staining results correlated with TAU Ab-3 immunostaining (Figure 6A) and thioflavin-S-staining (data not shown), whereas no $A\beta$ deposits could be observed in these regions.

These findings have been confirmed within the investigation of olfactory epithelium tissue of 20 confirmed AD patients (classification analysis: NIA Reagan Institute criteria²⁷) in comparison to 5 healthy controls. The severity of tau load in the Bowman's glands and its correlation to the progress of AD is subject to ongoing investigation. These results hold potential to detect AD-related tau deposits endoscopically and, therefore, noninvasively in the olfactory epithelium at very high resolution. The advantages of such a method compared to imaging techniques based on radiotracers, which require elaborate infrastructure and on-site radiochemical synthesis of suitable tracers, are apparent. Moreover, the diameter of a Bowman's gland is ~ 50 μm , which is far below the resolution of PET or SPECT probes. These are thus limited to the quantification of an averaged protein deposition, which in turn is rather low prior to the onset of symptoms, resulting in a signal-to-noise limitation of these techniques.

The applied fluorescent markers for Bowman's gland imaging should display cell permeability whereas a brain penetration would no longer be necessary, since the olfactory bulb is not confined by the blood–brain barrier. A contamination of the brain by brain-penetrating markers and their metabolites may be avoided, since tracers as **5** clear from the brain extremely slowly and can still be detected 100 days post injection (pi) at barely diminished intensity compared to day 1 pi.¹⁰

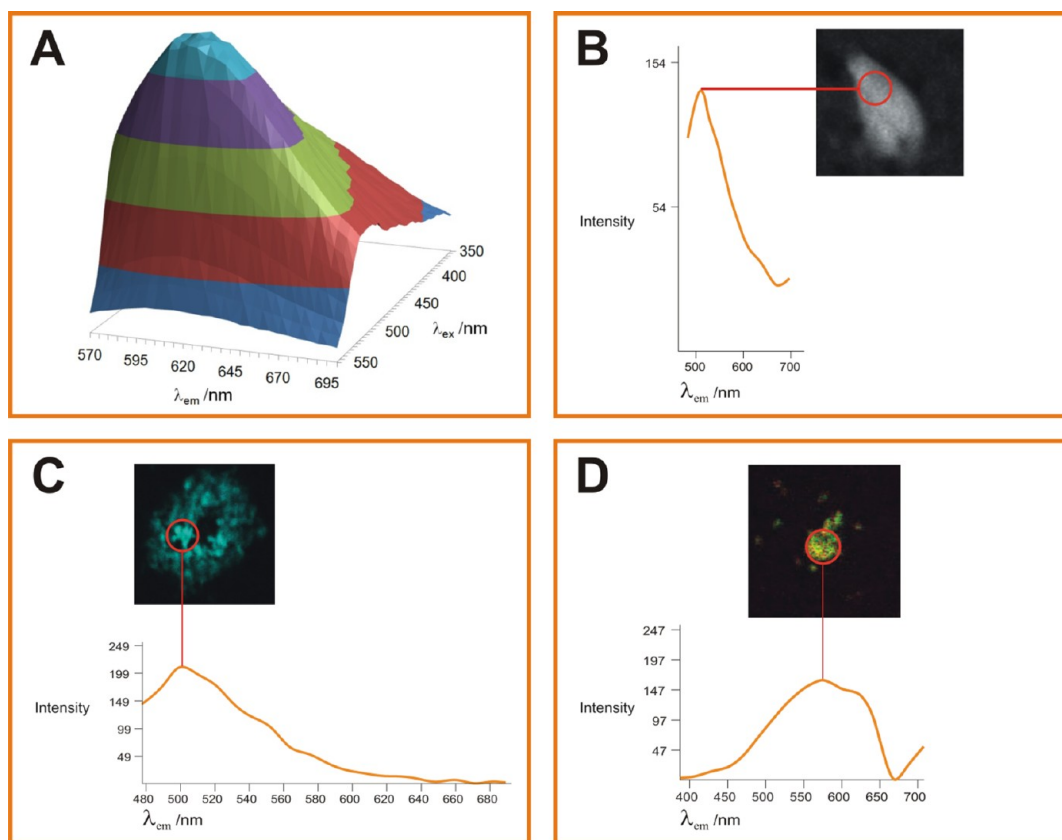


Figure 5. (A) 2D absorption/emission spectra of 7a (measured in methanol). (B–D) In vitro on target emission spectra of 7a on human hippocampal tissue [(B) tau fibril; (C) $A\beta$ plaque; (D) lipofuscin].¹³

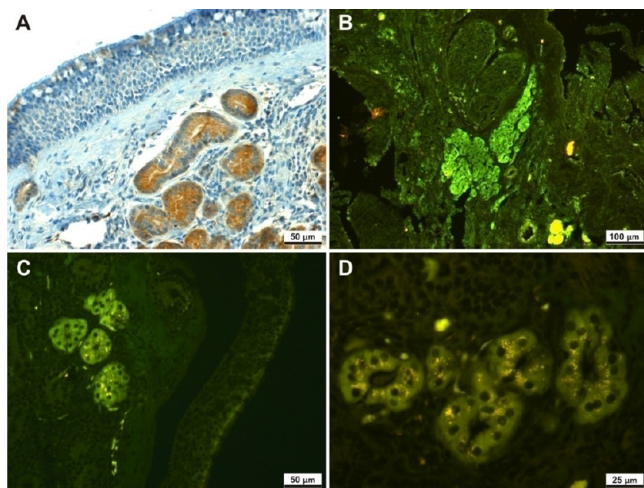


Figure 6. Bowman's glands of the olfactory epithelium containing tau aggregates extracted from a deceased AD patient (88y, Braak V, CERAD C): (A) immunohistological staining with antibody TAU Ab-3; (B) stained with 7a; (C and D) stained with 6a.^{13,15}

EXPERIMENTAL SECTION

General Information. All chemicals were purchased as reagent grade from commercial suppliers and used without further purification, unless otherwise noted. Proton (^1H NMR) and carbon (^{13}C NMR) nuclear magnetic resonance spectra were recorded on Bruker DRX 500 at 500 and 125.75 MHz, respectively, at 293 K. The chemical shifts are given in parts per million (ppm) on the delta scale (δ) and are referenced to tetramethylsilane ($\delta = 0$ ppm), ^1H NMR. Abbreviations for NMR data: s = singlet; d = doublet; t = triplet; q

= quartet; qi = quintet; dd = doublet of doublets; dt = doublet of triplets; dq = doublet of quartets; tt = triplet of triplets; m = multiplet. Coupling constants (J values) are given in hertz (Hz). Mass spectra were recorded on a Finnigan MAT 95 magnetic sector spectrometer. Thin-layer chromatography (TLC) was performed using Merck TLC silica gel 60 F 254 (0.2 mm) on aluminum sheets. Silica gel columns for chromatography were prepared with E. Merck silica gel 60 (0.063–0.20 mesh ASTM). UV/vis-spectra in methanolic solution were recorded using a Shimadzu UV-2401 PC UV-vis recording spectrometer; fluorescence spectra in methanolic solution were recorded using a Shimadzu RF-1501 spectrofluorophotometer. 2D fluorescence spectra were recorded on a Tecan Inffite M1000.

High-performance liquid chromatographies (HPLC) were carried out on an Agilent 1100 (column: reversed phase, Zorbax Eclipse XDB-C18, 4.6 mm \times 150 mm; detector: Agilent 1100 series refractive index detector, 254 nm). Solvent gradient = 90% A at 0 min, 30% A at 2 min, 10% A at 5 min; solvent A = 0.1% trifluoroacetic acid in water; solvent B = acetonitrile; flow rate = 1.0 mL/min; temperature = 35 $^\circ\text{C}$.

All compounds that were evaluated in biological assays had >95% purity, which has been determined using this method.

Synthesis of Bis(arylvinyl)pyrazines (6a–h) and Bis(arylvinyl)pyrimidines (7a–e). 2,5-Dimethylpyrazine (0.125 g, 1.16 mmol) or 4,6-dimethylpyrimidine (0.125 g, 1.16 mmol) was dissolved in 10 mL of dry dimethylformamide, potassium *tert*-butoxide (0.26 g, 2.31 mmol) was added, and the mixture was heated to 80 $^\circ\text{C}$. After 15 min, the corresponding aromatic aldehyde (2.31 mmol) was added and the reaction mixture was stirred for 4 h at 80 $^\circ\text{C}$. After cooling to ambient temperature, the resulting solid was filtered off and washed with ethyl acetate. If necessary, the obtained product was purified by column chromatography.

4,4'-(1*E*,1'*E*)-2,2'-(Pyrazine-2,5-diyl)bis(ethene-2,1-diyl)bis(*N,N*-dimethylaniline) (6a). Yield 0.370 g, 86%, red solid. ^1H NMR (CDCl_3 , 500 MHz): δ [ppm] = 3.02 (12H, s), 6.72 (4H, d, $J = 8.9$ Hz), 6.96 (2H, d, $J = 16$ Hz), 7.49 (4H, d, $J = 8.9$ Hz), 7.62 (2H, d, $J = 16$ Hz),

8.49 (2H, s). ^{13}C NMR (CDCl_3 , 125 MHz): δ [ppm] = 39.3, 111.2, 118.7, 123.7, 127.5, 132.8, 141.7, 148.0, 149.7. HPLC: 98%; t_{R} = 3.20 min. HRMS: calcd. for $\text{C}_{24}\text{H}_{26}\text{N}_4$, 370.2158; found, 370.21641.

2,5-Bis(*E*-2-(1-methyl-1*H*-pyrrol-2-yl)vinyl)pyrazine (6b). Yield 0.301 g, 89%, orange solid. ^1H NMR (CDCl_3 , 500 MHz): δ [ppm] = 3.76 (6H, s), 6.19 (2H, m), 6.65 (2H, m), 6.70 (2H, m), 6.88 (2H, d, J = 15.6 Hz), 7.62 (2H, d, J = 15.6 Hz), 8.40 (2H, s). ^{13}C NMR (CDCl_3 , 125 MHz): δ [ppm] = 33.3, 107.8, 107.9, 119.3, 120.6, 124.1, 130.5, 142.1, 147.8. HPLC: 96%; t_{R} = 7.53 min. HRMS: calcd. for $\text{C}_{18}\text{H}_{18}\text{N}_4$, 290.1532; found, 290.15118.

2,5-Bis(4-methoxystyryl)pyrazine (6c). Yield 0.322 g, 80%, yellow solid. ^1H NMR (CDCl_3 , 500 MHz): δ [ppm] = 3.85 (6H, s), 6.93 (4H, d, J = 9 Hz), 7.04 (2H, d, J = 16 Hz), 7.55 (4H, d, J = 9 Hz), 7.67 (2H, d, J = 16 Hz), 8.54 (2H, s). ^{13}C NMR (CDCl_3 , 125 MHz): δ [ppm] = 53.4, 112.3, 120.0, 126.7, 131.7, 141.0, 146.9, 158.3. HPLC: 99%; t_{R} = 4.63 min. HRMS: calcd. for $\text{C}_{22}\text{H}_{20}\text{N}_2\text{O}_2$, 344.1525; found, 344.15173.

2,5-Bis(4-isopropylstyryl)pyrazine (6d). Yield 0.373 g, 86%, light yellow solid. ^1H NMR (CDCl_3 , 500 MHz): δ [ppm] = 1.28 (12H, d, J = 6.9 Hz), 2.94 (2H, d, J = 6.9 Hz), 7.14 (2H, d, J = 16.1 Hz), 7.26 (4H, d, J = 8.1 Hz), 7.54 (4H, d, J = 8.1 Hz), 7.71 (2H, d, J = 16.1 Hz), 8.58 (2H, s). ^{13}C NMR (CDCl_3 , 125 MHz): δ [ppm] = 23.9, 34.0, 123.3, 127.0, 127.3, 134.0, 134.2, 143.1, 149.1, 150.0. HPLC: 97%; t_{R} = 5.25 min. HRMS: calcd. for $\text{C}_{26}\text{H}_{28}\text{N}_2$, 368.2253; found, 368.22192.

2,5-Bis(4-morpholinostyryl)pyrazine (6e). Yield 0.417 g, 79%, orange solid. ^1H NMR (CDCl_3 , 500 MHz): δ [ppm] = 3.25 (8H, t, J = 4.8 Hz), 3.90 (8H, t, J = 4.8 Hz), 6.95 (4H, d, J = 8.8 Hz), 7.03 (2H, d, J = 16.2 Hz), 7.53 (4H, d, J = 8.8 Hz), 7.66 (2H, d, J = 16.2 Hz), 8.53 (2H, s). HPLC: 99%; t_{R} = 7.35 min. HRMS: calcd. for $\text{C}_{28}\text{H}_{30}\text{N}_4\text{O}_2$, 454.2369; found, 454.2354.

2,5-Bis(4-(4-methylpiperazin-1-yl)styryl)pyrazine (6f). Yield 0.463 g, 83%, yellow solid. ^1H NMR (500 MHz, CDCl_3 , 300 K): δ [ppm] = 2.36 (s, 6H), 2.58 (8H, t, J = 5.0 Hz), 3.30 (8H, t, J = 5.0 Hz), 6.92 (4H, d, J = 8.8 Hz), 7.00 (2H, d, J = 16.1 Hz), 7.50 (4H, d, J = 8.8 Hz), 7.63 (2H, d, J = 16.1 Hz), 8.51 (2H, s). ^{13}C NMR (125 MHz, CDCl_3 , 300 K): δ [ppm] = 45.2, 47.3, 54.0, 114.4, 120.1, 126.4, 127.4, 132.6, 141.9, 148.0, 150.4. HPLC: 98%; t_{R} = 1.80 min. HRMS: calcd. for $\text{C}_{30}\text{H}_{34}\text{N}_6$, 480.3003; found, 480.30034.

2,5-Bis(4-(piperidin-1-yl)styryl)pyrazine (6g). Yield 0.413 g, 79%, orange solid. ^1H NMR (500 MHz, CDCl_3 , 300 K): δ [ppm] = 1.61 (4H, m), 1.70 (8H, m), 3.26 (8H, t, J = 5.3 Hz), 6.91 (4H, d, J = 8.5 Hz), 6.99 (2H, d, J = 15.9 Hz), 7.49 (4H, d, J = 8.5 Hz), 7.62 (2H, d, J = 15.9 Hz), 8.50 (2H, s). ^{13}C NMR (125 MHz, CDCl_3 , 300 K): δ [ppm] = 24.4, 25.6, 49.7, 115.6, 120.6, 126.7, 128.4, 133.7, 142.8, 149.0, 152.1. HPLC: 96%; t_{R} = 6.51 min. HRMS: calcd. for $\text{C}_{30}\text{H}_{34}\text{N}_4$, 450.2784; found, 450.27531.

2,5-Bis(4-(pyrrolidin-1-yl)styryl)pyrazine (6h). Yield 0.402 g, 82%, brown solid. ^1H NMR (500 MHz, CDCl_3 , 300 K): δ [ppm] = 2.03 (8H, m), 3.34 (8H, t, J = 6.6 Hz), 6.56 (4H, d, J = 8.7 Hz), 6.93 (2H, d, J = 16.0 Hz), 7.48 (4H, d, J = 8.7 Hz), 7.61 (2H, d, J = 16.0 Hz), 8.48 (2H, s). ^{13}C NMR (125 MHz, CDCl_3 , 300 K): δ [ppm] = 25.5, 47.6, 111.8, 119.0, 123.9, 128.7, 134.0, 142.7, 149.0, 151.3. HPLC: 99%; t_{R} = 6.28 min. HRMS: calcd. for $\text{C}_{28}\text{H}_{30}\text{N}_4$, 422.2471; found, 422.24976.

4,4'-(1*E*,1'*E*)-2,2'-(Pyrimidine-4,6-diyl)bis(ethene-2,1-diyl)bis(*N,N*-dimethylaniline) (7a). Yield 0.383 g, 89%, yellow solid. ^1H NMR (500 MHz, CDCl_3 , 300 K): δ [ppm] = 2.93 (12H, s), 6.62 (4H, d, J = 8.6 Hz), 6.76 (2H, d, J = 15.8 Hz), 7.06 (1H, s), 7.42 (4H, d, J = 8.6 Hz), 7.73 (2H, d, J = 15.8 Hz), 8.90 (1H, s). ^{13}C NMR (125 MHz, CDCl_3 , 300 K): δ [ppm] = 40.6, 112.4, 115.4, 121.2, 124.2, 129.5, 137.6, 151.5, 158.5, 163.4. HPLC: 98%; t_{R} = 6.35 min. HRMS: calcd. for $\text{C}_{24}\text{H}_{26}\text{N}_4$, 370.2158; found, 370.21534.

4,6-Bis(4-morpholinostyryl)pyrimidine (7b). Yield 0.464 g, 88%, yellow solid. ^1H NMR (500 MHz, CDCl_3 , 300 K): δ [ppm] = 3.24 (8H, t, J = 5.0 Hz), 3.87 (8H, t, 5.0 Hz), 6.91 (4H, d, J = 8.9 Hz), 6.91 (2H, d, J = 15.9 Hz), 7.20 (1H, s), 7.53 (4H, d, J = 8.9 Hz), 7.82 (2H, d, J = 15.9 Hz), 9.03 (1H, s). ^{13}C NMR (125 MHz, CDCl_3 , 300 K): δ [ppm] = 48.4, 66.7, 115.0, 115.7, 122.8, 127.0, 129.0, 136.6, 151.9,

158.6, 163.0. HPLC: 96%; t_{R} = 6.48 min. HRMS: calcd. for $\text{C}_{28}\text{H}_{30}\text{N}_4\text{O}_2$, 454.2369; found, 454.23502.

4,6-Bis(4-(4-methylpiperazin-1-yl)styryl)pyrimidine (7c). Yield 0.468 g, 84%, yellow solid. ^1H NMR (500 MHz, CDCl_3 , 300 K): δ [ppm] = 2.35 (6H, s), 2.57 (8H, t, J = 5.1 Hz), 3.30 (8H, t, J = 5.1 Hz), 6.89 (2H, d, J = 15.9 Hz), 6.91 (4H, d, J = 8.8 Hz), 7.19 (1H, s), 7.51 (4H, d, J = 8.8 Hz), 7.81 (2H, d, J = 15.9 Hz), 9.02 (1H, s). ^{13}C NMR (125 MHz, CDCl_3 , 300 K): δ [ppm] = 45.2, 47.1, 48.0, 53.9, 114.2, 114.5, 121.2, 121.6, 125.6, 128.0, 135.6, 150.8, 157.6, 162.0. HPLC: 99%; t_{R} = 1.80 min. HRMS: calcd. for $\text{C}_{30}\text{H}_{36}\text{N}_6$, 480.3003; found, 480.29930.

4,6-Bis(4-(piperidin-1-yl)styryl)pyrimidine (7d). Yield 0.481 g, 92%, yellow solid. ^1H NMR (500 MHz, CDCl_3 , 300 K): δ [ppm] = 1.60 (8H, t, J = 4.1 Hz), 1.68 (8H, m), 3.27 (8H, t, J = 5.8 Hz), 6.88 (2H, d, J = 15.9 Hz), 6.90 (4H, d, J = 8.8 Hz), 7.18 (1H, s), 7.50 (4H, d, J = 8.8 Hz), 7.80 (2H, d, J = 15.9 Hz), 9.00 (1H, s). ^{13}C NMR (125 MHz, CDCl_3 , 300 K): δ [ppm] = 24.3, 25.6, 49.5, 115.3, 115.4, 122.0, 125.8, 129.0, 136.8, 152.5, 158.5, 163.1, 170.6. HPLC: 98%; t_{R} = 5.20 min. HRMS: calcd. for $\text{C}_{30}\text{H}_{34}\text{N}_4$, 450.2784; found, 450.27606.

4,6-Bis(4-(pyrrolidin-1-yl)styryl)pyrimidine (7e). Yield 0.422 g, 86%, brown solid. ^1H NMR (500 MHz, CDCl_3 , 300 K): δ [ppm] = 2.02 (8H, t, J = 6.5 Hz), 3.34 (8H, t, J = 6.5 Hz), 6.56 (4H, d, J = 8.8 Hz), 6.82 (2H, d, J = 15.9 Hz), 7.14 (1H, s), 7.50 (4H, d, J = 8.8 Hz), 7.80 (2H, d, J = 15.9 Hz), 8.97 (1H, s). ^{13}C NMR (125 MHz, CDCl_3 , 300 K): δ [ppm] = 25.5, 47.6, 111.7, 115.0, 120.4, 123.1, 129.3, 137.2, 148.6, 158.5, 163.2. HPLC: 96%; t_{R} = 5.07 min. HRMS: calcd. for $\text{C}_{30}\text{H}_{34}\text{N}_4$, 422.2471; found, 422.24958.

4,4'-(1*E*,1'*E*,3*E*,3'*E*)-4,4'-(Pyrimidine-4,6-diyl)bis(buta-1,3-diene-4,1-diyl)bis(*N,N*-dimethylaniline) (7f). Yield 0.358 g, 73%, red solid. ^1H NMR (500 MHz, CDCl_3 , 300 K): δ [ppm] = 2.93 (12H, s), 6.41 (2H, d, J = 15.1 Hz), 6.61 (4H, d, J = 8.7 Hz), 6.75 (4H, d, J = 5.1 Hz), 6.98 (1H, s), 7.31 (4H, d, J = 8.7 Hz), 7.57 (2H, m), 8.90 (1H, s). ^{13}C NMR (125 MHz, CDCl_3 , 300 K): δ [ppm] = 39.3, 111.2, 114.3, 122.5, 123.9, 126.0, 127.3, 137.2, 137.7, 149.7, 157.5, 161.8. HPLC: 99%; t_{R} = 5.88 min. HRMS: calcd. for $\text{C}_{28}\text{H}_{30}\text{N}_4$, 422.2471; found, 422.24540.

Synthesis of Dimethyl 4-Arylpyridazine-3,6-dicarboxylates (14a–c). Dimethyl 4-arylpyridazine-3,6-dicarboxylates (14a–c) were obtained according to a published procedure.¹²

Dimethyl 4-Phenylpyridazine-3,6-dicarboxylate (14a). Yield 3.302 g, 96%, brown solid. ^1H NMR (500 MHz, CDCl_3 , 300 K): δ [ppm] = 3.87 (3H, s), 4.10 (3H, s), 7.56 (5H, m), 8.27 (1H, s). ^{13}C NMR (125 MHz, CDCl_3 , 300 K): δ [ppm] = 53.3, 53.6, 127.9, 128.2, 129.2, 130.2, 133.9, 140.0, 151.7, 154.3, 164.1, 165.5. EI-MS: m/z = 272 [M]⁺.

Dimethyl 4-(4-Methoxyphenyl)pyridazine-3,6-dicarboxylate (14b). Yield 0.751 g, 74%, yellow solid. ^1H NMR (500 MHz, CDCl_3 , 300 K): δ [ppm] = 3.86 (3H, s), 3.90 (3H, s), 4.09 (3H, s), 8.23 (1H, s), 7.39 (2H, d, J = 8.9 Hz), 7.01 (2H, d, J = 8.9 Hz). ^{13}C NMR (125 MHz, CDCl_3 , 300 K): δ [ppm] = 53.3, 53.6, 55.5, 114.8, 125.9, 127.8, 129.6, 139.5, 151.6, 154.3, 161.4, 164.2, 165.9. EI-MS: m/z = 302 [M]⁺.

Dimethyl 4-(2-Fluorophenyl)pyridazine-3,6-dicarboxylate (14c). Yield 1.07 g, 73%, brown solid. ^1H NMR (500 MHz, CDCl_3 , 300 K): δ [ppm] = 3.93 (3H, s), 4.10 (3H, s), 7.25 (4H, m), 8.26 (1H, s). ^{13}C NMR (125 MHz, CDCl_3 , 300 K): δ [ppm] = 53.3, 53.6, 115.9, 122.4, 125.0, 129.4, 130.1, 132.2, 135.6, 151.9, 153.4, 159.0, 163.6, 164.7. EI-MS: m/z = 290 [M]⁺.

Synthesis of (4-Arylpyridazine-3,6-diyl)dimethanols (15a–c). 4-Arylpyridazine-3,6-diyl dimethanols (15a–c) were obtained according to a published procedure.¹²

(4-Phenylpyridazine-3,6-diyl)dimethanol (15a). Yield 0.551 g, 51%, brown oil. ^1H NMR (CDCl_3 , 300 MHz, 300 K): δ [ppm] = 3.22 (2H, s), 4.88 (2H, s), 5.04 (2H, s), 7.47 (1H, s), 7.41 (5H, m). ^{13}C NMR (CDCl_3 , 125 MHz, 300 K): δ [ppm] = 61.8, 63.5, 125.1, 128.3, 129.1, 129.6, 134.5, 140.2, 157.5, 161.0. EI-MS: m/z = 216 [M]⁺.

(4-(4-Methoxyphenyl)pyridazine-3,6-diyl)dimethanol (15b). Yield 0.948 g, 77%, brown oil. ^1H NMR (CDCl_3 , 300 MHz, 300 K): δ [ppm] = 3.22 (2H, s), 3.92 (3H, s), 4.88 (2H, s), 5.04 (2H, s), 7.02 (2H, d, J = 9.0 Hz), 7.51 (1H, s), 7.55 (2H, d, J = 9.0 Hz). ^{13}C NMR

(CDCl₃, 125 MHz, 300 K): δ [ppm] = 53.4, 62.9, 66.4, 114.6, 126.2, 132.8, 135.2, 141.3, 156.9, 158.4, 161.2. EI-MS: m/z = 246 [M]⁺.

(4-(2-Fluorophenyl)pyridazine-3,6-diyl)dimethanol (15c). Yield 0.761 g, 65%, brown oil. ¹H NMR (CDCl₃, 300 MHz, 300 K): δ [ppm] = 4.78 (2H, s), 4.99 (2H, s), 7.52 (4H, m), 7.58 (1H, s). ¹³C NMR (CDCl₃, 125 MHz, 300 K): δ [ppm] = 62.1, 64.0, 127.5, 127.9, 128.2, 128.3, 131.8, 132.9, 138.1, 141.9, 158.5, 161.2. EI-MS: m/z = 234 [M]⁺.

Synthesis of 3,6-Bis(chloromethyl)-4-arylpyridazines (16a–c). To a solution of the corresponding (4-arylpyridazine-3,6-diyl)-dimethanol (15a–c) (1.5 mmol) in dichloromethane, SOCl₂ (0.450 g, 3.75 mmol) was added, and the solution was stirred at ambient temperature for 20 min, during which its color changed from brown to dark red. After the addition of water and extraction with dichloromethane, the united organic layers were dried over sodium sulfate. The resulting product could be used for the next step without further purification.

3,6-Bis(chloromethyl)-4-phenylpyridazine (16a). Yield 0.114 g, 30%, red oil. ¹H NMR (CDCl₃, 300 MHz, 300 K): δ [ppm] = 4.84 (2H, s), 4.94 (2H, s), 7.41 (5H, m), 7.63 (1H, s). ¹³C NMR (CDCl₃, 125 MHz, 300 K): δ [ppm] = 42.7, 44.2, 127.1, 128.4, 129.0, 129.6, 134.9, 141.6, 156.8, 158.9. EI-MS: m/z = 253 [M]⁺.

3,6-Bis(chloromethyl)-4-(4-methoxyphenyl)pyridazine (16b). Yield 0.149 g, 35%, red oil. ¹H NMR (CDCl₃, 300 MHz, 300 K): δ [ppm] = 3.89 (3H, s), 4.86 (2H, s), 4.94 (2H, s), 7.06 (2H, d, J = 8.9 Hz), 7.47 (2H, d, J = 8.9 Hz), 7.60 (1H, s). ¹³C NMR (CDCl₃, 125 MHz, 300 K): δ [ppm] = 42.8, 44.1, 53.4, 127.4, 127.9, 129.2, 131.7, 135.0, 142.5, 153.8, 158.3. EI-MS: m/z = 283 [M]⁺.

3,6-Bis(chloromethyl)-4-(2-fluorophenyl)pyridazine (16c). Yield 0.317 g, 78%, brown oil. ¹H NMR (CDCl₃, 300 MHz, 300 K): δ [ppm] = 4.83 (2H, s), 4.92 (2H, s), 7.56 (4H, m), 7.61 (1H, s). ¹³C NMR (CDCl₃, 125 MHz, 300 K): δ [ppm] = 42.7, 44.2, 127.1, 128.4, 129.0, 129.2, 130.6, 131.1, 136.8, 142.3, 155.8, 160.9. EI-MS: m/z = 271 [M]⁺.

Synthesis of Tetraethyl (4-Arylpyridazine-3,6-diyl)bis(methylene)diphosphonates (17a–c). The corresponding dichloride (16a–c) (0.5 mmol) was dissolved in P(OEt)₃ (8.310 g, 50 mmol), and the mixture was stirred for 18 h at 110 °C whereupon the color of the solution changed from dark red to black. After cooling to room temperature, residual P(OEt)₃ was distilled off (high vacuum, 100 °C) and the diphosphonate was obtained as a highly viscous dark oil, which was used for the next step without further purification.

Tetraethyl (4-Phenylpyridazine-3,6-diyl)bis(methylene)diphosphonate (17a). Yield 0.21 g, 92%, dark brown oil. ¹H NMR (CDCl₃, 500 MHz, 300 K): δ [ppm] = 1.24 (6H, t, J = 7.1 Hz), 1.27 (6H, t, J = 7.1 Hz), 3.60 (2H, d, J = 20.97), 3.61 (2H, d, J = 21.9), 4.06 (4H, m), 4.10 (4H, m), 7.47 (6H, m). ¹³C NMR (CDCl₃, 125 MHz, 300 K): δ [ppm] = 16.2, 16.4, 31.5, 33.9, 62.3, 62.5, 128.0, 128.8, 128.9, 129.0, 135.9, 141.0, 152.9, 154.0. EI-MS: m/z = 456 [M]⁺.

Tetraethyl (4-(4-Methoxyphenyl)pyridazine-3,6-diyl)bis(methylene)diphosphonate (17b). Yield 0.163 g, 69%, dark brown oil. EI-MS: m/z = 486 [M]⁺.

Tetraethyl (4-(2-Fluorophenyl)pyridazine-3,6-diyl)bis(methylene)diphosphonate (17c). Yield 0.209 g, 88%, dark brown oil. EI-MS: m/z = 472 [M]⁺.

Synthesis of Bis(arylvinyl)pyridazines (8a–e). The corresponding tetraethyl (4-arylpyridazine-3,6-diyl)bis(methylene)diphosphonate (17a–c) (0.25 mmol) was dissolved in dry DMF, and NaH (0.024 g, 1 mmol) was added. After stirring for 30 min, a solution of the corresponding aldehyde (0.5 mmol) in dry DMF was added. After stirring for 18 h, 1 N HCl was added and the mixture was extracted with DCM. The united organic layers were washed with saturated brine and dried over sodium sulfate, and the solvent was evaporated. After column chromatography the products were obtained as colored solids.

4,4'-(1E,1'E)-2,2'-(4-Phenylpyridazine-3,6-diyl)bis(ethene-2,1-diyl)bis(N,N-dimethylaniline) (8a). Yield 0.035 g, 31%, red solid. ¹H NMR (CDCl₃, 500 MHz, 300 K): δ [ppm] = 2.98 (6H, s), 3.02 (6H, s), 6.66 (2H, d, J = 8.8 Hz), 6.73 (2H, d, J = 8.8 Hz), 6.94 (1H, d, J =

15.6 Hz), 7.26 (1H, d, J = 16.4 Hz), 7.37 (2H, d, J = 8.8 Hz), 7.42 (s, 1H), 7.49 (5H, m), 7.51 (2H, d, J = 8.8 Hz), 7.59 (1H, d, J = 16.4 Hz), 8.05 (1H, d, J = 15.6 Hz). ¹³C NMR (CDCl₃, 125 MHz, 300 K): δ [ppm] = 40.2, 40.3, 112.1, 112.3, 117.4, 120.5, 123.4, 124.5, 125.1, 128.6, 128.8, 128.9, 129.1, 129.2, 135.2, 136.9, 138.4, 138.7, 150.7, 150.9, 153.8, 156.1. HPLC: 98%; t_R = 6.88 min. HRMS: calcd. for C₃₀H₃₀N₄, 446.2471; found, 446.24664.

4,4'-(4,4'-(1E,1'E)-2,2'-(4-Phenylpyridazine-3,6-diyl)bis(ethene-2,1-diyl)bis(4,1-phenylene))dimorpholine (8b). Yield 0.050 g, 37%, red solid. ¹H NMR (CDCl₃, 500 MHz, 300 K): δ [ppm] = 3.19 (4H, t, J = 5.0 Hz), 3.23 (4H, t, J = 5.0 Hz), 3.86 (8H, m), 6.85 (2H, d, J = 9.0 Hz), 6.91 (2H, d, J = 9.0 Hz), 7.01 (1H, d, J = 15.8 Hz), 7.30 (1H, d, J = 16.3 Hz), 7.40 (2H, d, J = 9.0 Hz), 7.43 (1H, s), 7.45 (5H, m), 7.53 (2H, d, J = 9.0 Hz), 7.61 (1H, d, J = 16.3 Hz), 8.06 (1H, d, J = 15.8 Hz). ¹³C NMR (CDCl₃, 125 MHz, 300 K): δ [ppm] = 48.6, 48.6, 66.7, 115.1, 115.2, 119.1, 122.1, 123.6, 127.7, 128.2, 128.5, 128.6, 128.7, 128.9, 129.0, 129.3, 133.9, 134.8, 136.7, 138.5, 151.4, 151.5, 153.7, 156.1. HPLC: 99%; t_R = 7.18 min. HRMS: calcd. for C₃₄H₃₄N₄O₂, 530.2682; found, 530.26589.

3,6-Bis(4-(1-methyl-1H-pyrrol-2-yl)styryl)-4-phenylpyridazine (8c). Yield 0.036 g, 39%, orange solid. ¹H NMR (CDCl₃, 500 MHz, 300 K): δ [ppm] = 8.07 (d, J = 15.5 Hz, 1H), 7.84 (d, J = 15.9 Hz, 1H), 7.53–7.44 (m, 5H), 7.23 (s, 1H), 7.00 (d, J = 15.9 Hz, 1H), 6.89 (d, J = 15.5 Hz, 1H), 6.72 (m, 1H), 6.69–6.65 (m, 2H), 6.43 (m, 1H), 6.20 (m, 1H), 6.12 (m, 1H), 3.76 (s, 3H), 3.72 (s, 3H). ¹³C NMR (CDCl₃, 125 MHz, 300 K): δ [ppm] = 155.6, 153.4, 142.7, 136.6, 131.8, 131.3, 129.0, 128.8, 128.1, 125.2, 124.9, 124.4, 122.5, 121.4, 120.4, 118.3, 108.9, 108.8, 108.6, 108.5, 34.3, 34.2. HPLC: 97%; t_R = 6.63 min. HRMS: calcd. for C₂₄H₂₂N₄, 366.1845; found, 366.18023.

4,4'-(1E,1'E)-2,2'-(4-(4-Methoxyphenyl)pyridazine-3,6-diyl)bis(ethene-2,1-diyl)bis(N,N-dimethylaniline) (8d). Yield 0.043 g, 36%, light red solid. ¹H NMR (CDCl₃, 500 MHz, 300 K): δ [ppm] = 2.99 (6H, s), 3.02 (6H, s), 3.91 (3H, s), 6.67 (2H, d, J = 8.7 Hz), 6.73 (2H, d, J = 8.7 Hz), 6.98 (1H, d, J = 15.8 Hz), 7.04 (2H, d, J = 8.7 Hz), 7.22 (1H, d, J = 16.2 Hz), 7.38 (5H, m), 7.51 (2H, d, J = 8.7 Hz), 7.58 (1H, d, J = 16.2 Hz), 8.04 (1H, d, J = 15.8 Hz). ¹³C NMR (CDCl₃, 125 MHz, 300 K): δ [ppm] = 40.2, 40.3, 55.4, 112.2, 112.2, 114.2, 117.9, 120.9, 123.1, 124.6, 125.2, 128.5, 128.7, 129.2, 130.5, 133.9, 134.8, 137.8, 150.7, 150.8, 153.9, 156.2, 160.0. HPLC: 98%; t_R = 7.27 min. HRMS: calcd. for C₃₁H₃₂N₄O₁, 476.2577; found, 476.25247.

4,4'-(1E,1'E)-2,2'-(4-(2-Fluorophenyl)pyridazine-3,6-diyl)bis(ethene-2,1-diyl)bis(N,N-dimethylaniline) (8e). Yield 0.041 g, 35%, red solid. ¹H NMR (CDCl₃, 500 MHz, 300 K): δ [ppm] = 2.98 (6H, s), 3.02 (6H, s), 6.66 (2H, d, J = 8.8 Hz), 6.73 (2H, d, J = 8.8 Hz), 6.77 (1H, d, J = 15.7 Hz), 7.22 (1H, d, J = 16.4 Hz), 7.25 (6H, m), 7.42 (1H, s), 7.51 (2H, d, J = 8.8 Hz), 7.58 (1H, d, J = 16.4 Hz), 8.05 (1H, d, J = 15.7 Hz). HPLC: 96%; t_R = 6.74 min. HRMS: calcd. for C₃₀H₂₈N₄F₁, 463.2299; found, 463.22797.

Tissue Probe Preparation. Human hippocampal tissue fixed in 10% buffered formalin solution and embedded in paraffin was cut to 4 μ m sections in a microtome and mounted on standard microscope slides. Subsequent deparaffinization was carried out in xylol (15 min), ethanol 100% (10 min), ethanol 96% (10 min), and ethanol 70% (10 min). Until subsequent processing, the slides were stored in water.

Immunohistochemical Staining. Immunohistochemical staining was performed on 4 μ m sections by using a Ventana Benchmark automated stainer (Ventana, Tuscon, AZ) applying the antibodies anti-PHF-Tau clone AT8 mAb (Thermo Scientific Pierce Research Products, Rockford, IL), TAU Ab-3 (Neomarkers, Fremont, CA), and amyloid A4 (BAM10, Sigma, St. Louis, MO) and the Ultraview Universal DAB Detection Kit (Ventana, Tuscon, AZ).

Histochemical Staining with Fluorescent Dyes. The staining procedure comprises the following steps of brain section treatment: nucleus staining with acidic hematoxylin (10 min), blue annealing by water wash-up (5 min), application of the dye solution (2.5 mM) (10 min), ethanol wash-up, water bath (5 min), 1% acetic acid bath (15 min), water wash-up, and covering with standard glass covers.

Light Microscopy and Fluorescence Microscopy. Four μ m sections stained with fluorescence probes were analyzed by indirect fluorescence microscopy using an Axioskop microscope with a

HBO100 fluorescence illuminator (Carl Zeiss, Oberkochen, Germany) with the bandpass filter set 09 BP450-490, FT510, LP515, the filter set 02 G365, FT395, LP420, and the filter set 15 BP546, FT580, LP590 (all Carl Zeiss, Oberkochen, Germany). Digital image processing was done with a Leica DFC 300FX fluorescence camera (Leica Microsystems, Heerbrugg, CH) and the software ImageAccess Premium version 5 (Imagic AG, Galtbrugg, CH).

Thiazine Red Displacement Assay. Recombinant human microtubule associated tau protein purified from *E. coli* was aggregated at a concentration of 5 μM with arachidonic acid (100 μM) in Tris 10 mM, pH 8, 24 h at 37 $^{\circ}\text{C}$. Synthetic $\text{A}\beta_{40}$ was aggregated at a concentration of 50 μM with arachidonic acid (100 μM) in Tris 10 mM, pH 8, for 3 days at 37 $^{\circ}\text{C}$, under shaking at 150 rpm.

Thiazine red was added at the concentration corresponding to the K_d of the respective aggregated protein binding site to induce a fluorescent signal that can be inhibited by the addition of a displacer compound. (K_d for aggregated tau = 18 nM, and K_d for aggregated $\text{A}\beta$ = 49 nM.)

To determine the affinity of a displacer compound to the thiazine red binding sites of the aggregated proteins, the compound was added at different concentrations to the assay mixture ranging from 0.1 to 10 000 nM. For the inhibition curve, the compound was measured together with the aggregated proteins and thiazine red. The fluorescence of some dyes overlapped with the fluorescence of thiazine red when measured at 595 nm. Therefore, compounds were also measured together with the aggregated proteins, but without thiazine red (autofluorescence curve) (Figure 7). Net fluorescence was

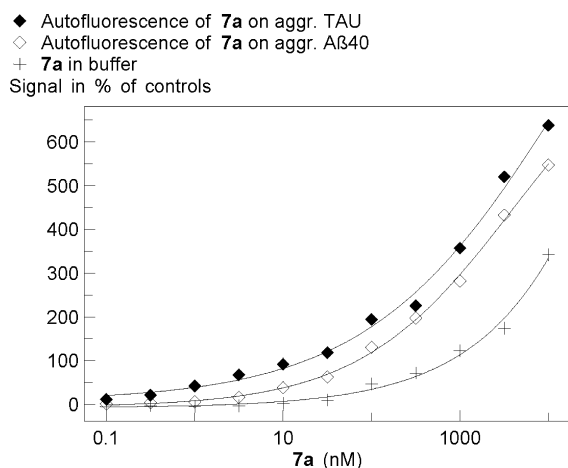


Figure 7. Fluorescence of 7a in buffer or in the presence of aggregated tau or aggregated $\text{A}\beta_{40}$.

calculated by subtracting the fluorescence of the wells without thiazine red from the fluorescence of wells containing thiazine red (inhibition curve) (Figure 8).

As negative control, thiazine red and aggregated protein were used. As positive control, thiazine red, reference compound with known activity (see Supporting Information, Table 1), and aggregated protein were used.

The assay was performed in Perkin-Elmer OptiPlate 384, black, 45 mL assay volume. As assay buffer, DPBS (no CaCl_2 , no MgCl_2) (GIBCO N. 14020) was used. The tested compounds were dissolved in dimethylsulfoxide (DMSO), and 2 μL of the solution was added to the assay mixture (5% DMSO final). The assay was started by the addition of the aggregated protein (competitive condition). The plates were shortly shaken (1 min with Sterico variomag telescope) and incubated at room temperature for 30 min. Measurements were performed with En:Vision (Perkin-Elmer), at excitation 531 nm/emission 595 nm. Corresponding IC_{50} values (inhibitory concentration for 50% decrease) were calculated using the Levenberg–Marquardt algorithm.¹³

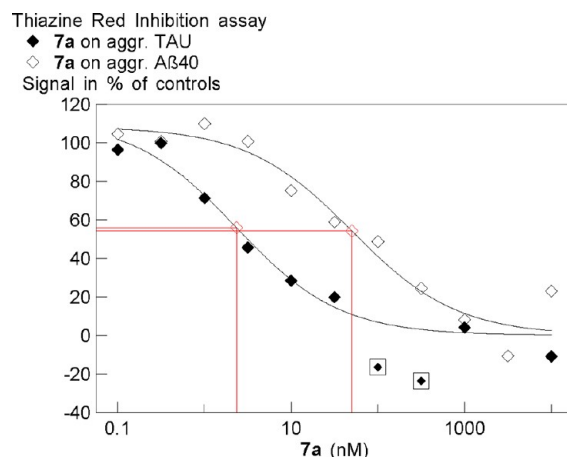


Figure 8. Inhibition curve in thiazine red assay of the compound 7a, with IC_{50} determination for aggregated tau and aggregated $\text{A}\beta_{40}$.

The obtained values are the average values of duplicates of replicate experiments. The statistical presentation follows the guidelines laid out by Cumming et al.²⁸

■ ASSOCIATED CONTENT

📄 Supporting Information

Immunohistochemical and histochemical staining, thiazine red displacement assay (further details), correlation of affinities to physicochemical parameters, toxicological evaluations of 7a and 7e, in vivo imaging, computational methods, and compound characterization data (original NMR spectra and HRMS protocols). This material is available free of charge via the Internet at <http://pubs.acs.org>.

■ AUTHOR INFORMATION

Corresponding Author

*Prof. Dr. Boris Schmidt, Clemens Schoepf-Institute of Organic Chemistry and Biochemistry, Technische Universität Darmstadt, Petersenstrasse 22, 64287 Darmstadt, Germany. E-mail: schmidt_boris@t-online.de. Phone: 49-6151 163075.

Author Contributions

The manuscript was written through contributions of all authors. All authors have given approval to the final version of the manuscript.

Notes

The authors declare the following competing financial interest(s): we claimed a patent application for the substances listed in this article, DE 10 2010 045 796.5, DE 10 2010 045 797.3, WO2012037928A2.

■ ACKNOWLEDGMENTS

This work was supported by the Bundesministerium fuer Bildung und Forschung, Germany (13N10636).

■ ABBREVIATIONS

α' , static electronic polarizability volume; α , calculated polarizability; CERAD, consortium to establish a registry for Alzheimer's disease; ϵ_0 , vacuum permittivity; ip, intraperitoneal injection; KOtBu , potassium *tert*-butoxide; K_d , dissociation constant; $\lambda_{\text{abs}}^{\text{max}}$, absorption maximum; $\lambda_{\text{em}}^{\text{max}}$, emission maximum; NIA, National Institute on Aging; *n.m.*, not measurable due to spectral overlap with the reference compound thiazine red; pi, post injection; y, years

■ REFERENCES

- (1) Wimo, A.; Winblad, B.; Aguero-Torres, H.; von Strauss, E. The magnitude of dementia occurrence in the world. *Alzheimer Dis. Assoc. Disord.* **2003**, *17*, 63–67.
- (2) Gandy, S. Perspective: Prevention is better than cure. *Nature* **2011**, *475*, S15.
- (3) Gravitz, L. Drugs: A tangled web of targets. *Nature* **2011**, *475*, S9–S11.
- (4) Klunk, W. E.; Engler, H.; Nordberg, A.; Wang, Y.; Blomqvist, G.; Holt, D. P.; Bergstrom, M.; Savitcheva, I.; Huang, G.-f.; Estrada, S.; Ausen, B.; Debnath, M. L.; Barletta, J.; Price, J. C.; Sandell, J.; Lopresti, B. J.; Wall, A.; Koivisto, P.; Antoni, G.; Mathis, C. A.; Langstrom, B. Imaging brain amyloid in Alzheimer's disease with Pittsburgh compound-B. *Ann. Neurol.* **2004**, *55*, 306–319.
- (5) Narlawar, R.; Pickhardt, M.; Leuchtenberger, S.; Baumann, K.; Krause, S.; Dyrks, T.; Weggen, S.; Mandelkow, E.; Schmidt, B. Curcumin-derived pyrazoles and isoxazoles: Swiss army knives or blunt tools for Alzheimer's disease? *ChemMedChem* **2008**, *3*, 165–172.
- (6) Ono, M.; Hayashi, S.; Matsumura, K.; Kimura, H.; Okamoto, Y.; Ihara, M.; Takahashi, R.; Mori, H.; Saji, H. Rhodanine and thiohydantoin derivatives for detecting tau pathology in Alzheimer's Brains. *ACS Chem. Neurosci.* **2011**, *2*, 269–275.
- (7) Koronyo-Hamaoui, M.; Koronyo, Y.; Ljubimov, A. V.; Miller, C. A.; Ko, M. K.; Black, K. L.; Schwartz, M.; Farkas, D. L. Identification of amyloid plaques in retinas from Alzheimer's patients and noninvasive in vivo optical imaging of retinal plaques in a mouse model. *NeuroImage* **2011**, *54*, S204–S217.
- (8) Klunk, W. E.; Bacskaï, B. J.; Mathis, C. A.; Kajdasz, S. T.; McLellan, M. E.; Frosch, M. P.; Debnath, M. L.; Holt, D. P.; Wang, Y.; Hyman, B. T. Imaging A β plaques in living transgenic mice with multiphoton microscopy and methoxy-X04, a systemically administered Congo red derivative. *J. Neuropathol. Exp. Neurol.* **2002**, *61*, 797–805.
- (9) Sadowski, M.; Pankiewicz, J.; Scholtzova, H.; Tsai, J.; Li, Y.; Carp, R. I.; Meeke, H. C.; Gambetti, P.; Debnath, M.; Mathis, C. A.; Shao, L.; Gan, W.-B.; Klunk, W. E.; Wisniewski, T. Targeting prion amyloid deposits in vivo. *J. Neuropathol. Exp. Neurol.* **2004**, *63*, 775–784.
- (10) Burgold, S.; Bittner, T.; Dorostkar Mario, M.; Kieser, D.; Fuhrmann, M.; Mitteregger, G.; Kretzschmar, H.; Schmidt, B.; Herms, J. In vivo multiphoton imaging reveals gradual growth of newborn amyloid plaques over weeks. *Acta Neuropathol.* **2011**, *121*, 327–335.
- (11) Achelle, S.; Nouira, I.; Pfaffinger, B.; Ramondenc, Y.; Ple, N.; Rodriguez-Lopez, J. V-shaped 4,6-bis(arylvinyl)pyrimidine oligomers: Synthesis and optical properties. *J. Org. Chem.* **2009**, *74*, 3711–3717.
- (12) Boger, D. L.; Panek, J. S.; Patel, M. Preparation and Diels–Alder reaction of a reactive, electron-deficient heterocyclic azadiene: Dimethyl 1,2,4,5-tetrazine-3,6-dicarboxylate. 1,2-Diazine (dimethyl 4-phenyl-1,2-diazine-3,6-dicarboxylate) and pyrrole (dimethyl 3-phenyl-pyrrole-2,5-dicarboxylate) introduction. *Org. Synth.* **1992**, *70*, 79–88.
- (13) See Supporting Information for further details.
- (14) cLogP values were determined using the OSIRIS Property Explorer: <http://www.organic-chemistry.org/prog/peo/>.
- (15) Tissue specimens were obtained with patients' informed consent in the course of regular clinical autopsies performed at the Department of Pathology, Klinikum Darmstadt.
- (16) Uchihara, T.; Nakamura, A.; Yamazaki, M.; Mori, O.; Ikeda, K.; Tsuchiya, K. Different conformation of neuronal tau deposits distinguished by double immunofluorescence with AT8 and thiazin red combined with Gallyas method. *Acta Neuropathol.* **2001**, *102*, 462–466.
- (17) Mohorko, N.; Repovs, G.; Popovic, M.; Kovacs, G. G.; Bresjanac, M. Curcumin labeling of neuronal fibrillar tau inclusions in human brain samples. *J. Neuropathol. Exp. Neurol.* **2010**, *69*, 405–414.
- (18) Bancher, C.; Brunner, C.; Lassmann, H.; Budka, H.; Jellinger, K.; Wiche, G.; Seitelberger, F.; Grundke-Iqbal, I.; Iqbal, K.; Wisniewski, H. M. Accumulation of abnormally phosphorylated τ precedes the formation of neurofibrillary tangles in Alzheimer's disease. *Brain Res.* **1989**, *477*, 90–99.
- (19) Kung, M.-P.; Hou, C.; Zhuang, Z.-P.; Skovronsky, D.; Kung, H. F. Binding of two potential imaging agents targeting amyloid plaques in postmortem brain tissues of patients with Alzheimer's disease. *Brain Res.* **2004**, *1025*, 98–105.
- (20) Luna-Munoz, J.; Peralta-Ramirez, J.; Chavez-Macias, L.; Harrington Charles, R.; Wischik Claude, M.; Mena, R. Thiazin red as a neuropathological tool for the rapid diagnosis of Alzheimer's disease in tissue imprints. *Acta Neuropathol.* **2008**, *116*, 507–515.
- (21) Mena, R.; Edwards, P.; Perez-Olvera, O.; Wischik, C. M. Monitoring pathological assembly of tau and β -amyloid proteins in Alzheimer's disease. *Acta Neuropathol.* **1995**, *89*, 50–56.
- (22) Schafer Kelsey, N.; Kim, S.; Matzavinos, A.; Kuret, J. Selectivity requirements for diagnostic imaging of neurofibrillary lesions in Alzheimer's disease: A simulation study. *NeuroImage* **2012**, *60*, 1724–1733.
- (23) Jensen, J. R.; Cisek, K.; Honson, N. S.; Kuret, J. Ligand polarizability contributes to tau fibril binding affinity. *Bioorg. Med. Chem.* **2011**, *19*, 5147–5154.
- (24) All procedures were in accordance with an animal protocol approved by the University of Munich and the government of upper Bavaria (Az. 55.2-1-54-2531-188-09).
- (25) Zhang, W.; Arteaga, J.; Cashion, D. K.; Chen, G.; Gangadharmath, U.; Gomez, L. F.; Kasi, D.; Lam, C.; Liang, Q.; Liu, C.; Mocharla, V. P.; Mu, F.; Sinha, A.; Szardenings, A. K.; Wang, E.; Walsh, J. C.; Xia, C.; Yu, C.; Zhao, T.; Kolb, H. C. A highly selective and specific PET tracer for imaging of tau pathologies. *J. Alzheimer's Dis.* **2012**, DOI: 10.3233/JAD-2012-120712.
- (26) Jung, T.; Bader, N.; Grune, T. Lipofuscin: Formation, distribution, and metabolic consequences. *Ann. N.Y. Acad. Sci.* **2007**, *1119*, 97–111.
- (27) Newell, K. L.; Hyman, B. T.; Growdon, J. H.; Hedley-Whyte, E. T. Application of the National Institute on Aging (NIA)–Reagan Institute criteria for the neuropathological diagnosis of Alzheimer disease. *J. Neuropathol. Exp. Neurol.* **1999**, *58*, 1147–1155.
- (28) Cumming, G.; Fidler, F.; Vaux, D. L. Error bars in experimental biology. *J. Cell Biol.* **2007**, *177*, 7–11.